



Investigation of indiscriminate nudging and predictability in a nested quasi-geostrophic model

Hiba Omrani,* Philippe Drobinski and Thomas Dubos

Institut Pierre Simon Laplace, Laboratoire de Météorologie Dynamique, École Polytechnique/ENS/UPMC/CNRS, Palaiseau, France

*Correspondence to: H. Omrani, Institut Pierre Simon Laplace/Laboratoire de Météorologie Dynamique, Ecole Polytechnique, F-91128, Palaiseau CEDEX, France. E-mail: hiba.omrani@lmd.polytechnique.fr

In this work, we consider the effect of indiscriminate nudging time on an idealized high-resolution global model (GM) and limited-area model (LAM) simulations. The model used is a two-layer quasi-geostrophic model on the beta-plane.

The effect of nudging is studied as a function of the predictability time, following a ‘Big Brother’ experimental approach: a high-resolution ‘global’ model is used to generate a ‘reference run’. These fields are filtered afterwards to remove small scales and provide the coarse-resolution fields which are used to drive the high-resolution GM and the LAM. Comparison of the reference fields and the high-resolution runs over the same region allows the estimation of the ability of the high-resolution GM and LAM to regenerate the removed small scales. This fully nonlinear set-up mimics the configuration used for regional high-resolution atmospheric modelling.

For the high-resolution GM, the results show that the behaviour of the nudged model depends primarily on the ratio of the nudging time to the predictability time. When the nudging time is very small compared to the predictability time, the model reproduces the large scale used to drive the model. On the other hand, if the nudging time is close to or larger than the predictability time, the nudging effect is weak and both large and small scales are poorly reproduced compared to the reference fields. The best result is obtained with a nudging time close to half the predictability time. This technique clearly improves the model capacity to reproduce the reference fields.

For the high-resolution LAM, our results show that for a sufficiently small domain the simulation is largely controlled by the lateral boundary conditions (LBCs) and is quasi-insensitive to nudging. However, if the domain size exceeds a few Rossby radii, the high-resolution LAM becomes sensitive to initial conditions and the control exerted by LBCs becomes insufficient to prevent a divergence from the driving fields. Although the reconstructed fine scales are significantly damped, they are surprisingly well correlated to their reference values in a deterministic sense, not a statistical sense. Copyright © 2011 Royal Meteorological Society

Key Words: downscaling; uncertainties; large/small-scale perturbations; potential vorticity

Received 9 July 2010; Revised 4 May 2011; Accepted 6 July 2011; Published online in Wiley Online Library 22 August 2011

Citation: Omrani H, Drobinski P, Dubos T. 2011. Investigation of indiscriminate nudging and predictability in a nested quasi-geostrophic model. *Q. J. R. Meteorol. Soc.* **138**: 158–169. DOI:10.1002/qj.907

1. Introduction

Atmosphere is one of the most challenging geophysical systems to simulate because of the number of interacting components and the wide range of time and spatial scales of relevant processes and their complexity. Spatial scales also vary greatly, ranging from the micro scale of cloud droplets to the planetary scale of the atmospheric circulation. Numerical modelling constitutes a powerful approach to further our understanding of the mechanisms responsible for the maintenance of the atmospheric system's dynamic equilibrium and variability, and to probe its response to changes in its external forcing. To date, general circulation models (GCM), used to simulate climate or provide analyses or reanalyses of the atmosphere, resolve only the broader scales of atmospheric circulations (around 100 km grid resolution). Hence there is a need to develop tools for downscaling the large-scale fields to generate finer-scale description of regional weather and climate. The starting point of dynamical downscaling is typically a set of coarse-resolution large-scale fields which are either used to drive a high-resolution GCM or to provide the initial, and lateral and surface boundary conditions to a nested limited area model (LAM).

Both GCMs and LAMs are sensitive to the resolution and to the content of physical parametrizations, and require a spin-up. LAMs also present specific issues like sensitivity to the size of the domain of simulation, to the boundary conditions, and to the frequency of update of boundary conditions (Bhaskaran *et al.*, 1996; Seth and Giorgi, 1998; Noguera *et al.*, 1998; Denis *et al.*, 2002a, 2003). For long-term simulations, Lo *et al.* (2008) showed that continuous runs can produce a very low score when the simulations are compared to observations and that simulations reinitialized periodically have better results than continuous runs. The practical solution to this issue is to explicitly disallow large and unrealistic departures between the coarse-resolution driving fields and the high-resolution fields by nudging the model towards the coarse-resolution driving fields. Nudging consists in adding to the conservation equations a Newtonian relaxation towards the driving fields.

Hence experience shows that, in order to reproduce a given weather history over a long period of time, a circulation model needs not only to be properly initialized but also to be nudged. Our basic hypothesis to explain this fact is that the need to nudge a high-resolution model results from its limited predictability. Indeed it is well known that atmospheric dynamics are sensitive to initial conditions (Thompson, 1957; Lorenz, 1963). Due to this inherent unpredictability of the atmosphere, small differences between a non-nudged model and the targeted state of the atmosphere amplify exponentially with time so that, after a finite time referred to as the predictability time, the model diverges from its target. In the specific case of a LAM it would seem that nudging is not necessary since the model is controlled by its lateral boundary conditions, which coincide with the targeted state of the atmosphere. The need to nudge would therefore indicate that it is not fully controlled by its lateral boundaries. In fact, since for a given model a specific simulation is entirely determined by the initial and boundary conditions, the amount of control exerted by the boundaries can be estimated by analysing the sensitivity of the model to initial conditions. Hence it appears that, for both GCMs and LAMs, the lack of predictability

due to sensitivity to initial conditions is intimately related to the practice of nudging towards driving fields.

Indiscriminate and spectral nudging is increasingly implemented in numerical models (GCM and LAM) (e.g. Kuo and Williams, 1992a, 1992b; Miguez-Macho *et al.*, 1992; von Storch *et al.*, 2000; Biner *et al.*, 2002; Genthon *et al.*, 2002; Lo *et al.*, 2008; Salameh *et al.*, 2010). Indiscriminate nudging was originally developed for assimilation issues (Davies and Turner, 1977; Schraff, 1997; Li *et al.*, 1998; Vidard *et al.*, 2003) but has become increasingly popular to drive Regional Climate Models (RCMs). The term 'indiscriminate nudging' is thus not as commonly used as 'spectral nudging'. Salameh *et al.* (2010) use the term 'indiscriminate nudging', Anthes (1974), Hoke and Anthes (1976) and Stauffer and Seaman (1990) refer to 'data assimilation', and other synonymous terminologies exist such as 'dynamical relaxation' (Davies and Turner, 1977) or 'grid' or 'analysis nudging'. In the following we will use 'indiscriminate nudging'.

Both indiscriminate and spectral nudging require that some relaxation time constant be adjusted. Indiscriminate nudging has been widely used for testing purposes, sensitivity studies, assimilation, and mesoscale or boundary layer studies (e.g. Vidard *et al.*, 2003; Lo *et al.*, 2008; Salameh *et al.*, 2010) and also for regional climate variability investigations (e.g. Genthon *et al.*, 2002; Coindreau *et al.*, 2007, with the global stretched grid regional model LMDZ; and Zhang *et al.*, 2009, with the limited area model WRF). Nudging techniques have demonstrated their usefulness in simulating regional weather and climate, especially in regions where forcing due to complex orography, or coastlines, regulates the spatial distribution of atmospheric variables (Raluca Rad *et al.*, 2008), especially orographic precipitation (Schraff, 1997; Tang *et al.*, 2010) and regional-scale climate variability (Genthon *et al.*, 2002; Coindreau *et al.*, 2007).

Currently the relaxation time is chosen based on trial and error and a posteriori validation rather than a priori understanding leading to suitable values. One key issue of this work is to explore the possibility of relating a tunable parameter to physical processes. The relation between the predictability time-scale τ_p and the relaxation time-scale τ is therefore investigated in this article. To test this hypothesis we adopt an approach similar to Salameh *et al.* (2010). In that study, the impact of nudging on a high-resolution model was investigated using a toy model consisting of resolving a linear transport equation with a Newtonian relaxation term. The toy model suffers from the same drift phenomenon as a complex atmospheric model and needs to be nudged as well. Salameh *et al.* (2010) predict the existence of an optimal nudging time which depends on the time-scale over which numerical errors affect significantly the accuracy of the solution at large spatial scales, and the typical time-scale of small-scale phenomena that are not resolved in the coarse-resolution driving fields. However, since the toy model is linear, its drift is solely due to accumulating numerical errors and not to a genuine unpredictability. To overcome this limitation we base our analysis on a two-layer quasi-geostrophic (QG) model which presents more similarities to atmospheric dynamics. We use a 'Big Brother' (BB) experimental approach, where the true atmospheric state is known, unlike when RCMs are used in practice (Denis *et al.*, 2002b). We address the relationship between nudging and predictability in two steps:

1. We first consider the relationship between nudging and predictability by using a refined 'global' QG model

as a high-resolution GCM. We especially investigate the ability of the high-resolution GCM to produce the correct small scales depending on the nudging time and predictability time.

2. We investigate the additional effect on predictability and nudging of lateral boundaries using a limited-area QG model as an LAM. This study is complementary to the few studies investigating the predictability of LAMs (Anthes *et al.*, 1985, 1989; Errico and Baumhefner, 1987; Van Tuyl and Errico, 1989; Vukicevic and Paegle, 1989; Vukicevic and Errico, 1990; De Elia *et al.*, 2002). By using a strongly idealized model we are able to explore a wide parameter space in terms of regional domain size and of nudging time.

Indiscriminate nudging is available in many up-to-date regional numerical models, such as the limited-area models MM5 (Grell *et al.*, 1995), WRF (Skamarock *et al.*, 2005), Méso-NH (Lafore *et al.*, 1998) and RAMS (Pielke *et al.*, 1992), and the global stretched grid regional model LMDZ (Gentson *et al.*, 2002; Coindreau *et al.*, 2007). For these reasons, and also for simplicity, we focus here on indiscriminate nudging. Spectral nudging is the object of ongoing work.

This paper is organized as follows. A description of the ‘global’ and ‘limited-area’ two-layer QG models and predictability issues is given in section 2. Downscaling using a high-resolution GCM is investigated in section 3, and the results from downscaling using a high-resolution LAM version are presented and discussed in section 4. Section 5 summarizes the results and points out some open research questions needing further investigation.

2. The quasi-geostrophic model

2.1. Equations

We use the flat-bottom two-layer quasi-geostrophic (QG) model on a β -plane derived by Haidvogel and Held (1980), modifying it only to implement a limited-area version, and include nudging terms. For completeness we reproduce in this subsection the derivation by Haidvogel and Held (1980). The dimensional form of the equations of motion can be written:

$$\partial_t Q_1 + J(\Psi_1, Q_1) = -\nu \nabla^6 \Psi_1, \quad (1)$$

$$\partial_t Q_2 + J(\Psi_2, Q_2) = -\nu \nabla^6 \Psi_2 - \kappa \nabla^2 \Psi_2, \quad (2)$$

where the subscripts 1 and 2 refer to the upper and lower layers of the model, respectively. The quantities Ψ_i and Q_i are the stream function and potential vorticity (PV) for layer i , J is the horizontal Jacobian operator $J(\Psi_i, Q_i) = (\partial_x \Psi_i \partial_y Q_i - \partial_y \Psi_i \partial_x Q_i)$ and ∇^2 is the horizontal Laplacian operator $\nabla^2 \Psi_i = \Delta \Psi_i = \partial_x^2 \Psi_i + \partial_y^2 \Psi_i$. The two layers have the same depth H at rest. The quantity ν is a numerical diffusion preventing the build-up of enstrophy in high wave numbers and κ is a surface friction term. The wind components (u_i, v_i) are related to the stream function

through the diagnostic relations

$$Q_1 = \nabla^2 \Psi_1 + \beta y + \frac{1}{2R_d^2} (\Psi_2 - \Psi_1), \quad (3)$$

$$Q_2 = \nabla^2 \Psi_2 + \beta y + \frac{1}{2R_d^2} (\Psi_1 - \Psi_2), \quad (4)$$

$$(u_i, v_i) = \left(-\frac{\partial \Psi_i}{\partial y}, \frac{\partial \Psi_i}{\partial x} \right), \quad i = 1, 2. \quad (5)$$

In these equations, $R_d = (g' \frac{H}{2f_0})^{1/2}$ is the Rossby radius, $g' = g \frac{\Delta \theta}{\theta_0}$ is the reduced gravity, θ and θ_0 are the potential temperature and the reference potential temperature, respectively, and f_0 is the Coriolis parameter. The upward displacement η of the interface between the two layers is given by $\frac{f_0 \eta}{H} = \frac{1}{2R_d^2} (\Psi_2 - \Psi_1)$.

Equations (3) and (4) state that upper and lower layer PV are conserved following the horizontal flow, except for the effects of dissipative processes. These latter processes are assumed to act on the relative vorticity ($\Delta \Psi_i$, $i = 1, 2$) through a biharmonic lateral diffusion in layers 1 and 2 and a linear surface drag in layer 2 only with turbulent mixing ratio coefficients ν and κ , respectively. Following Haidvogel and Held (1980), we consider the horizontally uniform time-averaged temperature gradient (directed north–south) and zonal vertical shear. The mean velocity is confined to the upper layer, so that $\bar{U}_2, \bar{V}_2, \bar{V}_1 = 0$ and $\bar{U}_1 = U$, with \bar{U}_i, \bar{V}_i the mean zonal and meridional wind components, respectively:

$$\Psi_1(x, y, t) = -Uy + \psi_1(x, y, t), \quad (6)$$

$$\Psi_2(x, y, t) = \psi_2(x, y, t), \quad (7)$$

where ψ_i ($i = 1, 2$) is the deviation of the stream function from its time average, i.e. $\Psi_i(x, y, t) = \bar{\Psi}_i(x, y) + \psi_i(x, y, t)$. Similar notation is used for the other variables (e.g. the potential vorticity).

Non-dimensionalizing (x, y, t, ψ) by $(R_d, R_d, \frac{R_d}{U}, UR_d)$ (x and y are the zonal and meridional coordinates), the QG PV equations for the transient flow become

$$\partial_t \hat{q}_1 + J(\hat{\psi}_1, \hat{q}_1) = -\hat{\nu} \nabla^6 \hat{\psi}_1 + F_1, \quad (8)$$

$$\partial_t \hat{q}_2 + J(\hat{\psi}_2, \hat{q}_2) = -\hat{\nu} \nabla^6 \hat{\psi}_2 - \hat{\kappa} \nabla^6 \hat{\psi}_2 + F_2, \quad (9)$$

where the eddy potential vorticities are

$$\hat{q}_1 = \nabla^2 \hat{\psi}_1 + \frac{1}{2} (\hat{\psi}_2 - \hat{\psi}_1), \quad (10)$$

$$\hat{q}_2 = \nabla^2 \hat{\psi}_2 + \frac{1}{2} (\hat{\psi}_1 - \hat{\psi}_2). \quad (11)$$

The forcing terms

$$F_1 = -\partial_x \hat{q}_1 - \left(\hat{\beta} + \frac{1}{2} \right) \partial_x \hat{\psi}_1, \quad (12)$$

$$F_2 = - \left(\hat{\beta} + \frac{1}{2} \right) \partial_x \hat{\psi}_2, \quad (13)$$

represent the effects of the mean temperature and planetary vorticity gradients on the transient flow. All variables in Eqs (10)–(13) are non-dimensional. The parameters which appear in these equations are $\hat{\beta} = \beta \frac{R_d^2}{U}$, $\hat{\kappa} = \kappa \frac{R_d}{U}$ and $\hat{\nu} = \frac{\nu}{R_d^3 U}$. In the following, for sake of simplicity, the hats of non-dimensional variables will be omitted.

2.2. Numerical implementation of the global and limited area QG models

The temporal integration of the two-layer QG model is based on second-order spatial finite differences and a third-order Runge–Kutta explicit temporal scheme. With finite differences, it is easy to apply the same discretization in the global and limited-area model. The main tasks to be performed during a time step are the computation of the PV trends $\partial_t q_i$ given ψ_i and the inversion of the PV, e.g. the computation of the stream functions ψ_i given the PV fields q_i .

Computation of the PV trend involves discrete approximations of the Jacobian and Laplacian operators. For the Jacobian we use Arakawa's Jacobian, which preserves energy and potential enstrophy at the discrete level, preventing spurious energy transfers to small scales (Arakawa, 1966). The Laplacian is approximated using the standard five-point stencil. The iterated Laplacian is approximated by iterating this approximate operator.

In this study, we adopt the BB experimental approach (Denis *et al.*, 2002b). The first step consists of running a global high-resolution BB model to produce a high-resolution reference dataset (q_i^{ref} , $i = 1, 2$). Then, the small scales existing in that reference dataset are filtered out to generate a low-resolution dataset (q_i^{ana} , $i = 1, 2$). The filtering technique consists in applying a two-dimensional Fourier filter to q_i^{ref} and the ratio between the horizontal resolutions of q_i^{ref} to q_i^{ana} is hereafter referred to as α . The q_i^{ana} fields can be seen as analyses, reanalyses or coarse-resolution GCM outputs. The q_i^{ana} fields are used to initialize and drive another instance of the QG model ('Little Brother') running at the same resolution as the BB. This mimics the driving of a high-resolution GCM or LAM by coarse-resolution atmospheric fields. We will later refer to the high-resolution GCM or LAM as 'Little Brother' (LB). The BB reference dataset (before filtering) q_i^{ref} contains the small scales against which the LB small scales are then validated. This experimental framework is set up to evaluate the ability of the LB to accurately reproduce the fine-scale features present in the BB reference simulation.

Boundary conditions are periodic in the 'global' QG model. In the LAM, evaluating the Jacobian and iterated Laplacian requires values of ψ_i located in a so-called halo around the computational domain. These values are given by the 'analyses' ψ_i^{ana} . Inverting the PV means solving the linear system

$$\begin{pmatrix} L-1 & 1 \\ 1 & L-1 \end{pmatrix} \begin{pmatrix} \psi_1 \\ \psi_2 \end{pmatrix} = \begin{pmatrix} q_1 \\ q_2 \end{pmatrix}, \quad (14)$$

where L is the second-order finite-difference operator approximating the Laplacian. In the global model, system (14) is solved by performing a forward discrete Fourier transform, solving for each Fourier mode a 2×2 linear system, and performing a backward discrete Fourier transform.

In the limited-area model, system (14) is supplemented by the Dirichlet boundary conditions $\psi_i = \psi_i^{\text{ana}}$. This enforces the continuity of the pressure field across the domain boundary, as physically required. We solve for the deviation $\delta\psi_i = \psi_i - \psi_i^{\text{ana}}$. The right-hand side term of system (14) then becomes $q_i - q_i^{\text{ana}}$, where q_i^{ana} is the PV computed from ψ_i^{ana} . The deviation $\delta\psi_i$ satisfies the boundary condition

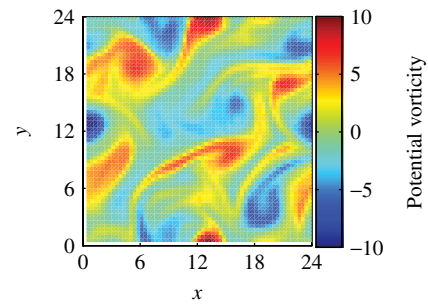


Figure 1. Horizontal cross-section of potential vorticity in layer 1 (q_1).

$\delta\psi_i = 0$. Therefore system (14) is solved by performing a forward discrete sine transform, solving for each Fourier mode a 2×2 linear problem, and performing a backward discrete sine transform. Finally, $\psi_i = \psi_i^{\text{ana}} + \delta\psi_i$ gives the desired ψ_i . Additionally, a relaxation over 6 points is applied at the boundaries, forming a Davies-type lateral sponge zone (we also performed the whole study without using a sponge zone, without noticeable change to the results; not shown). Figure 1 shows an example of a horizontal cross-section of the PV field in layer 1 of the model at long time range ($t > 20$ in non-dimensional units). It evidences the presence of anticyclones and cyclones of typical size equal to a few units (i.e. a few Rossby radii in dimensional form).

2.3. Nudged version of the QG model

As we analyse later in more detail, the simulated fields ψ_i deviate rapidly from the reanalyses ψ_i^{ana} if the latter are used only to prescribe boundary conditions. In order to prevent this drift, we use the nudging technique (or Newtonian relaxation) developed for assimilation purposes (Davies and Turner, 1977; Schraff, 1997; Yong *et al.*, 1998; Vidard *et al.*, 2003) and commonly available for dynamical downscaling purposes. The nudging technique consists of relaxing the model state towards the analyses by adding a non-physical term to the model equation. This nudging term is defined as the difference between the observation and the model solution, weighted by a nudging coefficient which is the inverse of the nudging time. After addition of the nudging term, Eqs (8) and (9) become

$$\partial_t q_1 + J(\psi_1, q_1) = -\nu \nabla^6 \psi_1 + F_1, \quad (15)$$

$$-\frac{1}{\tau}(q_1 - q_1^{\text{ana}}),$$

$$\partial_t q_2 + J(\psi_2, q_2) = -\nu \nabla^6 \psi_2 - \kappa \nabla^6 \psi_2 + F_2, \quad (16)$$

$$-\frac{1}{\tau}(q_2 - q_2^{\text{ana}}),$$

where the nudging time τ is a freely tunable parameter. The shorter the time τ , the closer q_i and ψ_i will be to q_i^{ana} and ψ_i^{ana} ($i = 1, 2$), and hence the less accurate the small scales of q_i will be.

To quantify the predictability time-scale τ_p in the QG models, we compute the initial exponential error growth, yielding the first Lyapunov exponent. We consider a run $\psi_i^1(t)$ and a second run called the perturbed simulation $\psi_i^2(t)$, which is almost identical except that its initial condition is different by a random and infinitesimal amount (10^{-3} amplitude Gaussian white noise). We compute the total energy of the difference between perturbed and

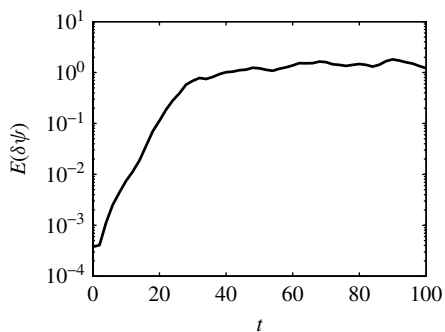


Figure 2. Evolution of total energy E of the difference between perturbed and reference stream functions as a function of normalized time t for $\beta = 0.25$ and $\kappa = 0.5$ (non-dimensional values).

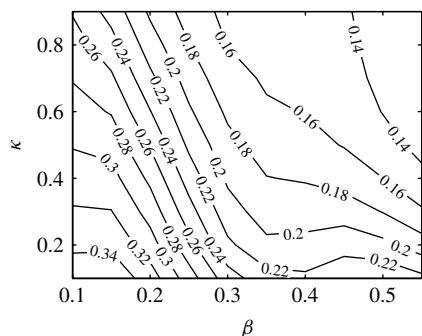


Figure 3. Contour plot of predictability time τ_p as a function of β and κ . The contours range between 0.14 and 0.34 with an increment of 0.2.

reference stream functions:

$$E(t) = \int \frac{\|\nabla\delta\psi_1\|^2 + \|\nabla\delta\psi_2\|^2}{2} dx dy + \int \left\| \left(\frac{\delta\psi_1 + \delta\psi_2}{2} \right)^2 \right\| dx dy, \quad (17)$$

where $\delta\psi_i = \psi_i^2 - \psi_i^1$.

The total energy E consists of the sum of upper and lower kinetic energies (first term of Eq. (17)) and potential energies (second term of Eq. (17)). Figure 2 displays a typical evolution of E as a function of time in log-scale along the ordinate axis. It clearly shows evidence of an exponential initial error growth (linear evolution in log-scale) until $t = 20$ in non-dimensional coordinates. Then there is nonlinear saturation. The exponential phase of error growth $E(t) = E_0 \exp(2\lambda t)$ defines the first Lyapunov exponent λ and the predictability time-scale $\tau_p = \frac{1}{\lambda}$.

Figure 3 shows the value of τ as a function β and κ . As also observed by Vallis (1983), the predictability properties of two-layer flow are rather subtly affected by β . Vallis (1983) argues that the energy cascade at low wavenumbers is slowed by a strong β , which increases predictability, whereas it weakly depends on κ . Similarly to Haidvogel and Held (1980), we set $\kappa = 0.5$ in the following and let β vary between 0.1 and 0.55.

3. Downscaling using a high-resolution GCM

In this section, we use the same periodic domain for BB and LB (Figure 4). One must note that downscaling by nudging a high-resolution GCM towards a coarse-resolution GCM

is of no practical use. The motivation is here to establish the relationship between the sensitivity to initial conditions and the nudging time in a context which is free of the technicalities associated with a LAM, which will be addressed in section 4.

To quantify the ability of the downscaled LB field q_i to reproduce the BB reference field q_i^{ref} in layer i , we first evaluate the variance ratio of LB to BB solutions $\sigma_{q_i}^2/\sigma_{q_i^{\text{ref}}}^2$. This is a classical diagnostic for climate model evaluation.

A second approach, which corresponds to deterministic evaluation, consists of computing their normalized covariance a_i given by

$$a_i = \frac{\text{cov}(q_i^{\text{ref}}, q_i)}{\sigma_{q_i^{\text{ref}}}^2}, \quad (18)$$

which represents the slope of the linear regression between q_i and q_i^{ref} (i.e. $q_i \sim a_i q_i^{\text{ref}} + b_i$), and the correlation coefficient r_i given by

$$r_i = \frac{\text{cov}(q_i^{\text{ref}}, q_i)}{\sigma_{q_i^{\text{ref}}} \sigma_{q_i}}, \quad (19)$$

with

$$\text{cov}(q_i^{\text{ref}}, q_i) = \frac{1}{N_x N_y} \sum_{k=1}^{N_x} \sum_{l=1}^{N_y} \left[q_i^{\text{ref}}(k, l) - \bar{q}_i^{\text{ref}} \right] \times \left[q_i(k, l) - \bar{q}_i \right], \quad (20)$$

$$\sigma_{q_i^{\text{ref}}} = \sqrt{\frac{1}{N_x N_y} \sum_{k=1}^{N_x} \sum_{l=1}^{N_y} \left[q_i^{\text{ref}}(k, l) - \bar{q}_i^{\text{ref}} \right]^2}, \quad (21)$$

$$\sigma_{q_i} = \sqrt{\frac{1}{N_x N_y} \sum_{k=1}^{N_x} \sum_{l=1}^{N_y} \left[q_i(k, l) - \bar{q}_i \right]^2}, \quad (22)$$

where \bar{q}_i^{ref} and \bar{q}_i are the values of q_i^{ref} and q_i averaged over the whole model domain in layer i . The quantities N_x , N_y are the number of grid points of the domain in the x (longitude) and y (latitude) directions. The quantities a_i and r_i represent the slope and spread of the scatter-plot between q_i^{ref} and q_i . When a_i and r_i are close to 1, the LB reproduces accurately at each time step and each grid point the BB reference field in layer i . Conversely, a large departure from 1 indicates poor LB performance. Therefore, a crucial aspect of the estimation of the LB performance in simulating the fine-scale features in the context of regional weather and climate modelling is the deterministic grid point to grid point comparison between the LB outputs q_i and the BB reference field q_i^{ref} . These skill scores are much more constraining than a comparison of climatological statistical diagnostics (Murphy and Epstein, 1989).

In the following, $\hat{\beta} = 0.25$; $\hat{\kappa} = 0.5$, $\hat{\nu} = 10^{-4}$. The domain size is $24R_d \times 24R_d$ and the number of grid points is 128×128 . This implies that one Rossby radius is made of 5.3 grid points. We run the LB model until $t = 100 \simeq 10\tau_p$ with different nudging time τ ranging between $0.01\tau_p$ and

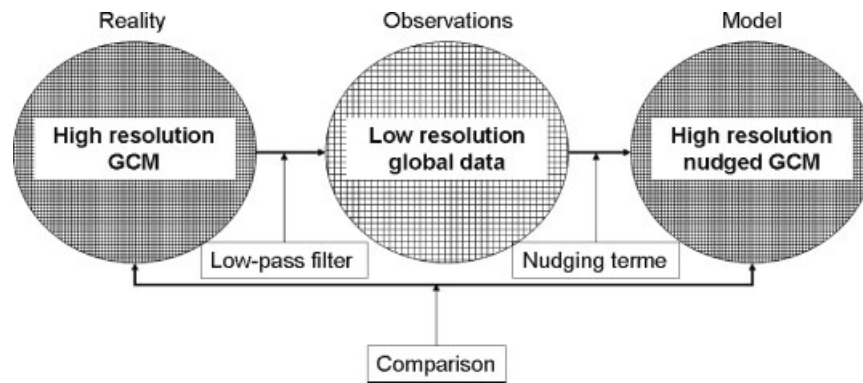


Figure 4. 'Big Brother' experiment principle using a high-resolution GCM.

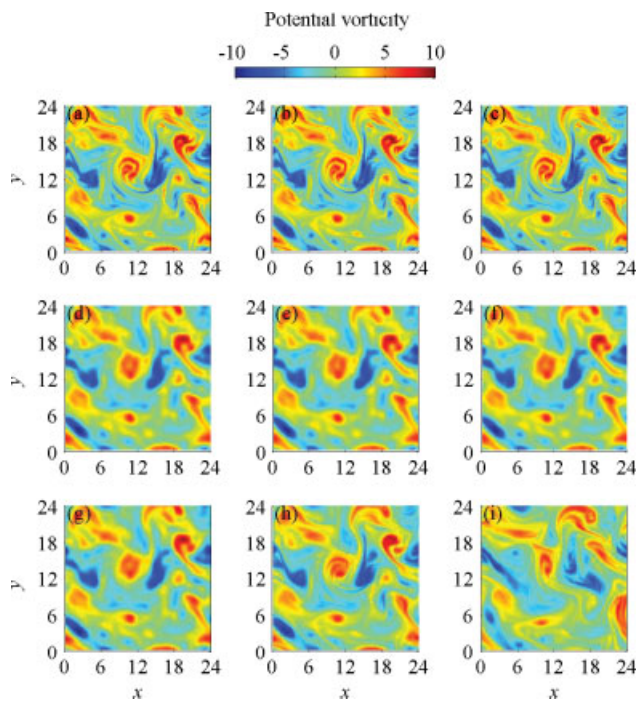


Figure 5. Horizontal cross-section of the reference (BB) PV in layer 1 (q_1^{ref}) (a, b, c), horizontal cross-section of the coarse-resolution driving PV in layer 1 obtained by filtering spatially the reference PV field (q_1^{ana}) (d, e, f) and horizontal cross-section of simulated (LB) PV in layer 1 (q_1) (g, h, i) for $\tau = 0.01\tau_p$ (a, d, g), $\tau = 0.4\tau_p$ (b, e, h) and $\tau = \tau_p$ (c, f, i). The ratio α between the horizontal resolutions of q_1^{ref} to q_1^{ana} is 1/3.

τ_p and a resolution factor α between 1/2 and 1/8. Figure 5 shows horizontal cross-sections in layer 1 at the end of the simulation of the reference (BB) PV q_1^{ref} , of the coarse-resolution driving PV q_1^{ana} obtained by spatially filtering q_1^{ref} with $\alpha = 1/3$ and of the simulated (LB) PV q_1 for $\tau = 0.01\tau_p$, $\tau = 0.4\tau_p$ and $\tau = \tau_p$, respectively.

A small value of the nudging time ($\tau = 0.01\tau_p$) forces the model to stick to the coarse-resolution driving fields: indeed, comparing Figure 5(g) (q_1) to Figure 5(d) (q_1^{ana}) and Figure 5(d) (q_1) to Figure 5(a) (q_1^{ref}), we can observe that the model reproduces perfectly the large-scale vortices but not the fine-scale structures. On the other hand, for $\tau = \tau_p$ (Figure 5(c, f, i)), the model is able to reproduce neither the large-scale nor the fine-scale features. The nudging time that corresponds to $\tau = 0.4\tau_p$ seems visually to be the optimum time since the model (Figure 5(h)) best agrees with the reference (Figure 5(b)).

In order to evaluate more quantitatively the quality of the simulations of the fine- and large-scale features, the LB PV fields q_i in the simulations are decomposed into a large-scale part ($q_{i,ls}$ and $q_{i,ls}^{ref}$) and a small-scale part ($q_{i,ss}$ and $q_{i,ss}^{ref}$) by application of low-pass and high-pass Fourier filters, with cut-off wavelength being the resolution of the field q_i^{ana} driving the simulation.

Figure 6 displays the variance ratio of LB to BB solutions averaged over $80 \leq t \leq 100$, as a function of the nudging time for the total field, large-scale field and small-scale field.

We note that for τ between 0 and $0.5\tau_p$, the amount of small scales increases until it reaches a maximum. It then decreases for τ between $0.5\tau_p$ and $6\tau_p$ down to a value of 0.2, and finally increases again up to about a value of 1. For small nudging time, the production of small-scale features is inhibited because by construction the model is forced to stick to the driving fields. Intuitively, we expect the production of the fine-scale features to be associated with increasing ratio of LB to BB solutions until it reaches 1 for large nudging time. This is not the case for τ between 0.5 and $6\tau_p$, where the ratio of LB to BB solutions decreases until it reaches a minimum. In fact, a similar behaviour is observed for the large-scale field. Hence nudging for this range of τ hinders the production of large-scale features too. To check the robustness of this result, a similar test was performed with the Lorenz model, which is much simpler than the QG model but still presents a chaotic character. The calculations showed a strongly reduced variance of the nudged model as well (not shown). The small variance of the small-scale BB flow compared to LB is probably the result of the weak large-scale LB flow. Finally, as expected, for very large values of τ , nudging no longer has any effect, and both the LB small- and large-scale fields have the same variance as in BB. One can note that the value of the ratio of LB to BB solutions slightly exceeds 1 for large τ . This is due to the uncertainty associated with the variance estimate for the two different fields. In the following we restrict the discussion to values of τ ranging between 0 and τ_p .

Figure 7 displays scatter-plots between the simulated (LB) and reference (BB) PV fields for $80 \leq t \leq 100$ in layer 1 for the large-scale ($q_{1,ls}$ and $q_{1,ls}^{ref}$) and for the small-scale ($q_{1,ss}$ and $q_{1,ss}^{ref}$) for $\tau = 0.01\tau_p$, $\tau = 0.4\tau_p$ and $\tau = \tau_p$.

For a small nudging time $\tau = 0.01\tau_p$ (Figure 7(a)), the LB large scale is accurately reproduced compared to the reference (BB) and the covariance and correlation coefficients $a_{1,ls}$ and $r_{1,ls}$ are $\simeq 1$. However, the LB small-scale features are very poorly reproduced as quantified with covariance and correlation coefficients $a_{1,ss} = 0.13$ and

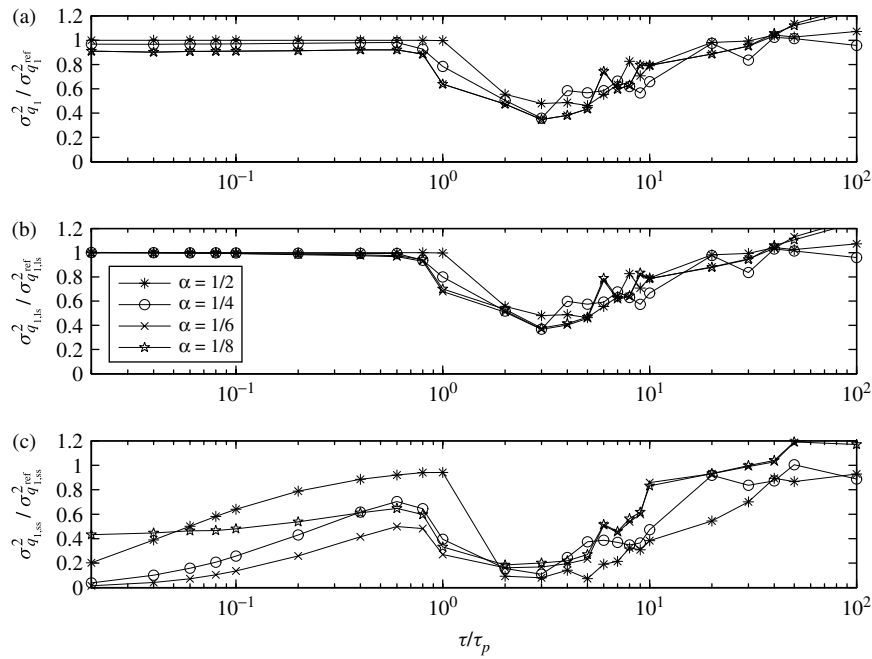


Figure 6. LB to BB ratio of averaged layer 1 PV variance, as a function of the nudging time τ normalized by τ_p (log scale) for the total field (a), large-scale field (b) and small-scale field (c). The different curves correspond to different resolution ratio α .

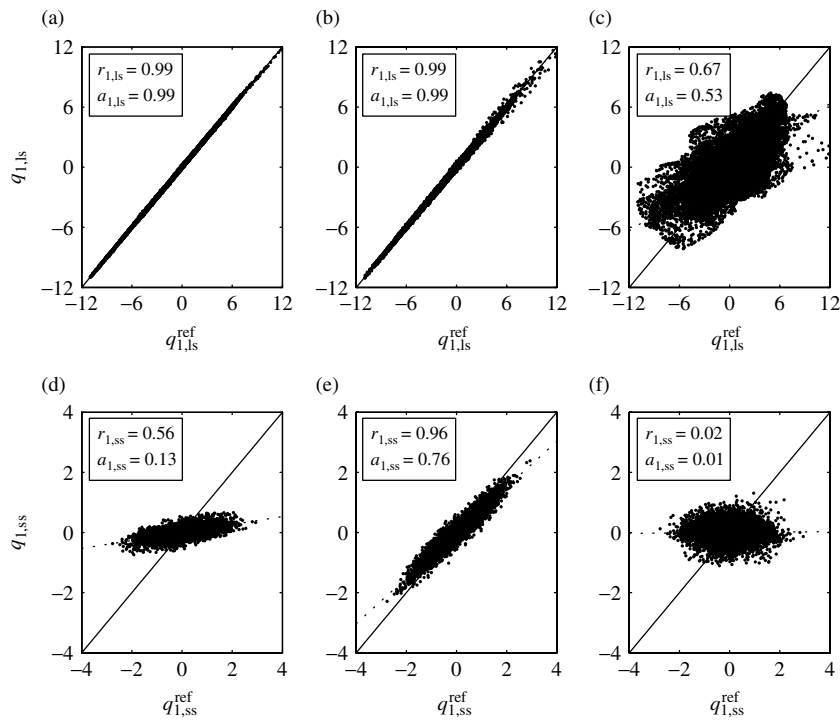


Figure 7. Scatter-plots between the simulated (LB) and reference (BB) PV fields in layer 1 for the large-scale ($q_{1,ls}$ and $q_{1,ls}^{ref}$) and for the small-scale ($q_{1,ss}$ and $q_{1,ss}^{ref}$) for $\tau = 0.01\tau_p$ (a, d), $\tau = 0.4\tau_p$ (b, e) and $\tau = \tau_p$ (c, f), respectively. The ratio α between the horizontal resolutions of q_i^{ref} to q_i^{ana} is $1/3$.

$r_{1,ss} = 0.56$ (Figure 7(d)). When τ is large, i.e. $\tau = \tau_p$, the error on the large scale increases significantly with $a_{1,ls} = 0.53$ and $r_{1,ls} = 0.67$ (Figure 7(c)) and induces large errors at the fine scale with $a_{1,ss} = 0.01$ and $r_{1,ss} = 0.02$ (Figure 7(f)). The use of the intermediate value of the nudging time $\tau = 0.4\tau_p$ allows the minimization of the error both at the small and large scales (Figure 7(b, e)). The covariance and correlation coefficients for the large scale $a_{1,ls}$ and $r_{1,ls}$ are ≈ 1 and for the small scale $a_{1,ss} = 0.76$ and $r_{1,ss} = 0.96$.

Figure 8 displays the covariance (a_1) and correlation (r_1) coefficients computed in layer 1 for the small (ss subscript) and the large scale (ls subscript) as a function of the nudging time normalized by the predictability time (τ/τ_p) using various resolution factors α .

The figure shows that for the large scale and for low to intermediate values of τ (from 0 to about $0.5\tau_p$), the covariance and correlation coefficients $a_{1,ls}$ and $r_{1,ls}$ remain very close to 1 because the relaxation is strong enough to prevent LB simulations (q_i) departing significantly from the

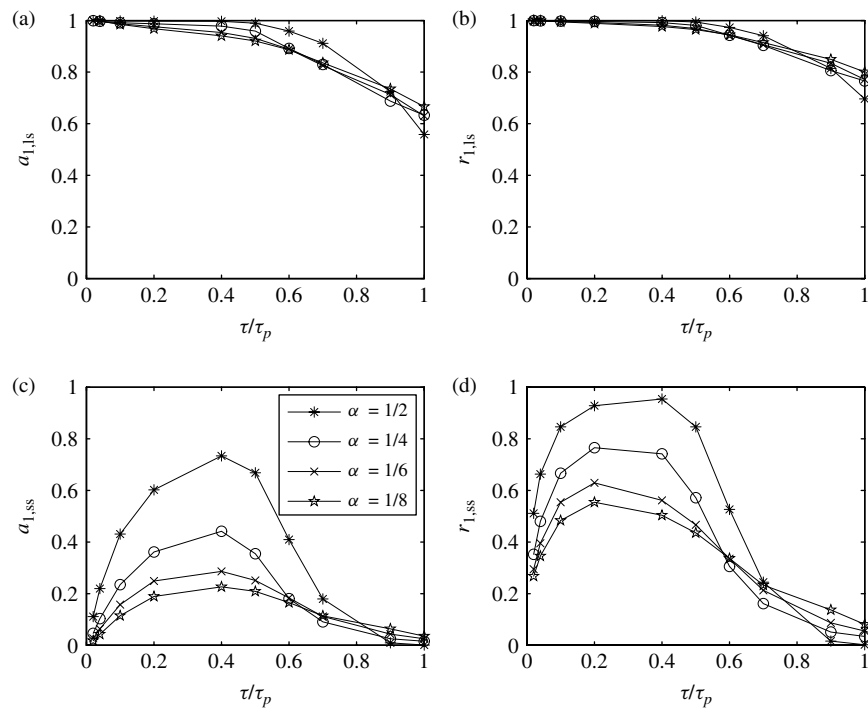


Figure 8. Covariance (a_1) (a, c) and correlation (r_1) (b, d) coefficients computed in layer 1 for the large (ls subscript, a, b) and small scales (ss subscript, c, d) as a function of the nudging time normalized by the predictability time (τ/τ_p) using various resolution factors α .

driving large-scale fields (q_i^{ana}) (Figure 8(a, b)). However, one can notice that for $\tau < 0.1\tau_p$ the small-scale field is very poorly simulated by LB and $a_{1,ss}$ and $r_{1,ss}$ reach maximum values between 0.1 and 0.5 (Figure 8(c, d)). Indeed, for such low values of τ the production of small-scale structures is inhibited because the LB fields are constrained by the nudging to match too tightly the coarse-resolution driving fields. As the nudging time increases ($\tau > 0.5\tau_p$), the model progressively deviates from the forcing large-scale fields. The LB does produce small-scale patterns, but they poorly match those present in the BB reference fields (Figure 5(i)). Indeed, $a_{1,ls}$ and $r_{1,ls}$ decrease below 0.6 and 0.8 respectively for the large scales and $a_{1,ss}$ and $r_{1,ss}$ tend to zero for the small scales. The departure of the LB large-scale fields from the coarse-resolution driving fields induces small-scale patterns that may be statistically representative of the mean regional climate (for $\tau/\tau_p > 10$; see Figure 6) but differ from the reference on a ‘grid point to grid point comparison’ basis. An optimum is eventually reached for intermediate values of τ , ranging between 0.3 and $0.6\tau_p$. Figure 8 also shows that LB simulations deteriorate when the resolution factor α decreases, i.e. the ratio between the resolution of the driving large-scale fields and the LB resolution increases. This deterioration is due to the too-coarse resolution the driving fields reach, which prevents the accurate representation of even the large-scale atmospheric circulation. This is especially critical when the driving field resolution becomes coarser than the Rossby deformation radius, corresponding roughly to $\alpha < 1/8$. Quantitatively, for $\tau = 0.4\tau_p$, $a_{1,ss}$ and $r_{1,ss}$ decrease from 0.73 and 0.95 for $\alpha = 1/2$ to 0.23 and 0.50 for $\alpha = 1/8$.

4. Downscaling using a high-resolution LAM

In this section, the main difference from section 3 is that we consider a limited-area model nested within the global

model, so that the size of the LAM domain L comes into play. The experimental framework of a perfect model used in this section is similar to that of the previous section but with a small modification (Figure 9): the first step consists of running the global high-resolution QG model, referred as ‘Big Brother’ (BB), to produce a high-resolution reference dataset ($q_i^{\text{ref}}, i = 1, 2$). Then, the small scales existing in that reference dataset are filtered out to generate a low-resolution dataset ($q_i^{\text{ana}}, i = 1, 2$) needed to drive the nested LAM. The q_i^{ana} fields are used as initial and boundary conditions of the LAM and to drive the LAM when nudging is used. The reference dataset (before filtering) q_i^{ref} contains the small scales against which the LAM small scales in the nested domain ($q_i, i = 1, 2$) are then validated. The performance of the LAM is quantified by the same parameters (a_i, r_i) as in the previous section, but in the nested domain only. We will later refer to the LAM as the ‘Little Brother’ (LB).

The effect of the LB domain size on the predictability is first investigated. For this the LAM is driven at its boundaries by the perfect data q_i^{ref} and initialized with perturbed data as described in section 3.2. No nudging is used. In Table I, the predictability time τ_p in normalized coordinate is reported as a function of the normalized domain size L/R_d .

We first observe that a finite predictability time is found for all the domain sizes we consider. If the simulation was completely controlled by its boundaries, the initial discrepancy between the reference and the perturbed simulations would decay as time passes and eventually vanish. Conversely, the finite predictability time of the LB implies that the control exerted by the boundary conditions is incomplete, in the sense that the trajectory followed by the model depends significantly on its initial condition, and not only on the information provided at the boundaries. We must, however, make clear here that the slower growth of initial errors in a small-domain LAM results from

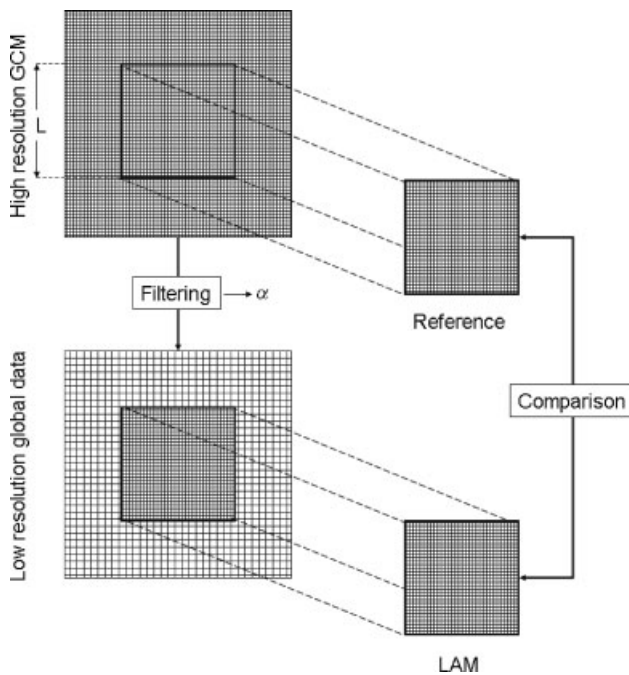


Figure 9. 'Big Brother' experiment approach using a LAM.

Table I. Predictability time τ_p as a function of the normalized domain size L/R_d .

| $N_x \times N_y$ | 64×64 | 80×80 | 96×96 | 112×112 |
|------------------|----------------|----------------|----------------|------------------|
| $\frac{L}{R_d}$ | 12 | 15 | 18 | 21 |
| τ_p | 18 | 15 | 13 | 10 |

the artificial constraints exerted by the lateral boundary conditions, and that it does not reflect a greater intrinsic predictability of the modelled atmosphere. However, for consistency with the previous section we keep referring to predictability when discussing the sensitivity to initial conditions.

The predictability decreases as the domain size of the LB increases. We interpret this dependency qualitatively in two ways. First, the characteristic size of a potential vorticity cyclone or anticyclone is comparable to the Rossby radius R_d . Then, as the domain size decreases, fewer cyclones and anticyclones fit into it. Therefore fewer interactions take place between the different cyclones and anticyclones, and predictability of the model increases. Second, as the domain size L decreases, an individual air parcel swept by the mean wind U spends a decreasing amount of time $\tau_{adv} = L/U$ in the domain. Assuming that the errors exit the domain as well, a small domain leaves them less time to develop than a large domain. Small domains can therefore be expected to lead to a more predictable system. Indeed, Vukicevic and Paegle (1989) show that if the domain is small enough the sensitivity of the forecast to small initial uncertainties is low. Similarly, Leduc and Laprise (2009) analysed the sensitivity of regional climate modelling to the domain size and showed that the small-scale stationary patterns improve in spatial correlation when the domain size is reduced. Conversely, Vannitsem and Chomé (2005) show that for a large domain a small error in initial condition leads to different simulations. The study of Alexandru *et al.* (2007) suggests that a reduction of

the domain size generally results in a significant reduction of LAM internal variability. Finally, Lucas-Picher *et al.* (2008) have computed the time spent by air parcels in the domain of an RCM. They find a linear relation between the spatial distribution of the internal variability and residency time. These previous results are fully consistent with a small domain having a larger predictability, and our postulated relationship between predictability and internal variability. Nutter *et al.* (2004) also show that the loss of dispersion within an ensemble of simulations is greater on smaller domains because features are advected more quickly from one side to the other.

Moreover, we have observed a complete suppression of sensitivity to initial conditions with a domain of size $L \leq 12R_d$ (i.e. smaller than 64×64 grid points). In an idealized set-up similar to ours, Nutter *et al.* (2004) address sensitivity to initial conditions by considering the internal variability within an ensemble of limited-area one-layer QG simulations on the β -plane. They also find that internal variability is smaller for small domains, with significant reduction for an LAM domain of size 1500 km (i.e. one R_d). Note that, owing to their use of a barotropic model instead of a baroclinic model like ours, we do not expect that the LAM domain size below which sensitivity to initial conditions disappears is the same.

We now consider nudging in a small domain of size $L = 12R_d$ for the LB, in a global domain of $24R_d$. The value of the predictability time τ_p is then 18 (Table I). Figure 10 displays the covariance and correlation coefficients computed in layer 1. The use of only 64×64 grid points makes the estimations of the covariance and correlation coefficients much noisier, especially for $\alpha < 1/4$. Nevertheless, one can see that, except for very low values of τ ($< 0.1\tau_p$), the values of the covariance and correlation coefficients are weakly dependent on the nudging time τ , so the quality and performance of the LB simulations do not depend on the strength of relaxation towards the coarse-resolution driving fields.

We finally consider a nudging in a larger domain of size $L = 18R_d$ for the LB, in a global domain of $24R_d$. The value of the predictability time τ_p is then 13 (Table I). Figure 11 displays the covariance and correlation coefficients computed in layer 1. The use of 96×96 grid points allows a more accurate estimate of the covariance and correlation coefficients, even though it is still noisier than with 128×128 grid points. The shape of the curves as a function τ_p is similar to that obtained with the high-resolution GCM, with a performance optimum for $\tau \simeq 0.4\tau_p$, but with slightly more spread between the various runs for different values of α (Figure 11). We see that, compared to the high-resolution GCM, the large scale is slightly less accurately reproduced. Also, the degradation of the performance with respect to α is larger, and for $\alpha < 1/4$ the small degradation of the LAM performance at a large scale does not allow the production of correct fine-scale features.

5. Discussion

When performing a dynamical downscaling experiment, one expects to produce data with two distinct improvements over the large-scale information. The first expectation is that the downscaled data will benefit from better-resolved forcings like orography and surface fluxes, which depend on spatially variable soil properties. The second

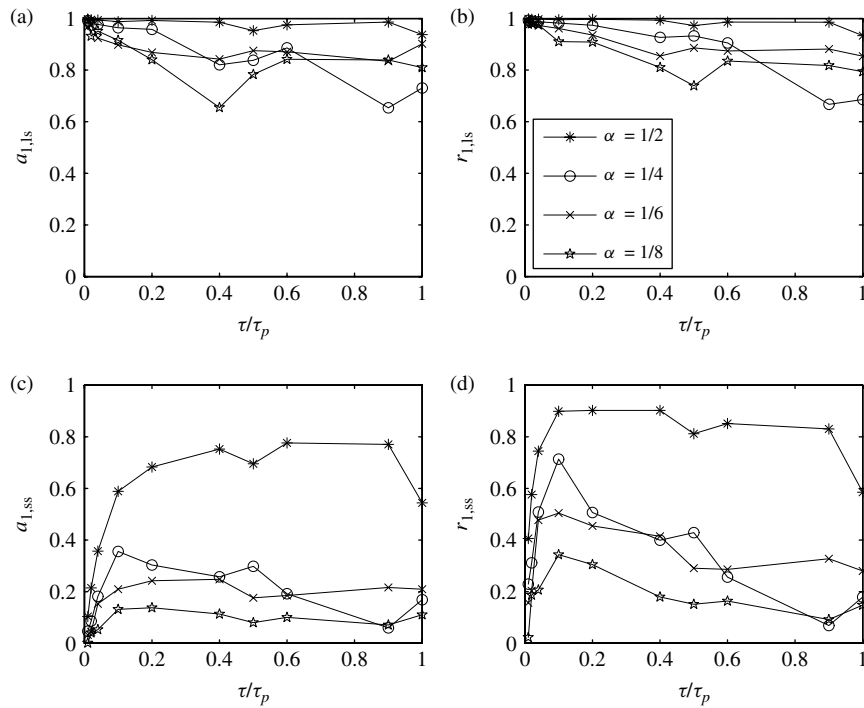


Figure 10. Covariance (a_1) (a, c) and correlation (r_1) (b, d) coefficients computed in layer 1 for the smallest LB domain— $N_x \times N_y = 64 \times 64$ i.e. $L = 12R_d$ (Table I)—for the large (ls subscript, a, b) and small scales (ss subscript, c, d) as a function of the nudging time normalized by the predictability time (τ/τ_p) using various resolution factors α .

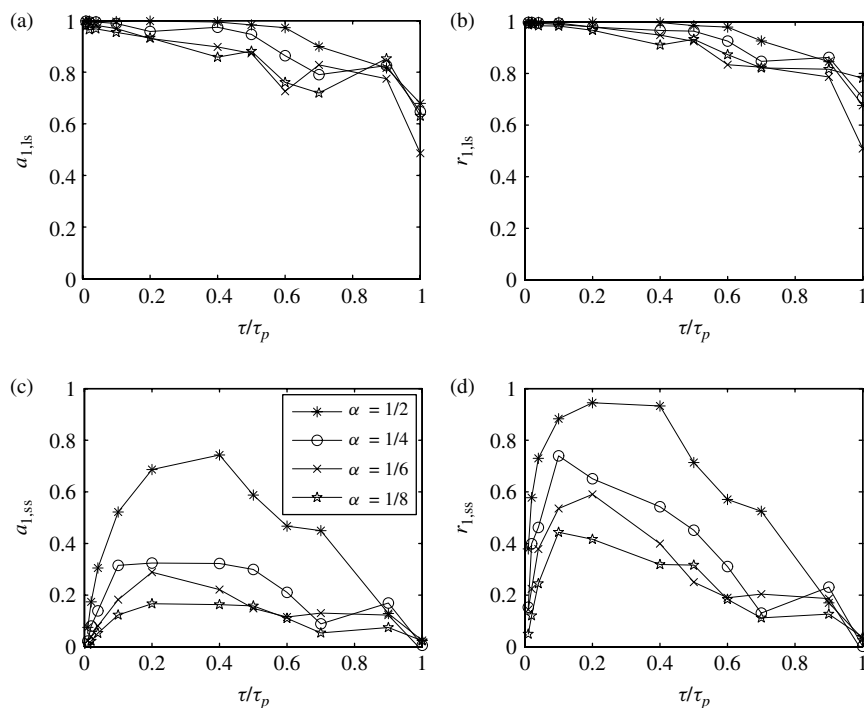


Figure 11. Same as Figure 10 for the LB domain— $N_x \times N_y = 96 \times 96$ i.e. $L = 18R_d$ (Table I).

expectation is that, even with orography and other boundary conditions unchanged, a simulation with higher resolution will produce smaller-scale eddies explicitly and take into account more accurately their contribution to the regional-scale averages and variability. Whether these expectations are realized can be investigated following the BB experimental approach, which has been used mostly with complex, realistic models and rarely with idealized models. With our idealized methodology, we are able to address the second

expectation independently from the first one. Furthermore, using an idealized model which nevertheless allows a good representation of the atmospheric dynamics driven by the baroclinic instability ensures that the results we obtain are a consequence of the resolved dynamics and not of some specific physical parameterization.

Since climate models forget rapidly about their initial conditions, it would seem that the concept of predictability is relevant to short-term weather forecasting but not to

long-term regional climate modelling. This will be the case if regional climate is studied using a standalone global model, but regional climate modelling is mostly done using LAMs. A LAM must maintain a consistency between the atmosphere it models within its domain and the fields that drive it at the boundary. This will not happen if the LAM is sensitive to initial conditions, since this implies that it is insufficiently controlled by its lateral boundaries. Our results show that LAMs with a domain larger than a few Rossby radii are sensitive to initial conditions even for perfect lateral boundary conditions, and therefore must be nudged in order to maintain their consistency with boundary data. Furthermore, the behaviour of the nudged model, both at large and small scales, depends primarily on the ratio of the nudging time to the predictability time.

When the nudging time is very small compared to the predictability time, the model reproduces the large scale used to force the model. On the other hand, if the nudging time is close to or larger than the predictability time, both large and fine scale are poorly reproduced compared to the reference fields. As a result, the internal variability of the model strongly depends on nudging. This technique clearly improves the model's capacity to reproduce the reference fields, used here as a surrogate for reality. The best result is obtained with a nudging time close to half the predictability time ($\tau = 0.4\tau_p$). Although the reconstructed fine scales are significantly damped, they are surprisingly well correlated to their reference values in a deterministic sense, not a statistical sense.

For LAM our predictability study shows that if the domain size increases the predictability of the system decreases. We speculate that when the LAM domain is sufficiently large the atmospheric system has more active parts in interaction, which increases its chaotic character and limits its predictability. Conversely, when the domain is small, the short time spent by air parcels in the domain does not allow initially present errors to develop. With nudging, the LAM capacity to reconstruct the small scales is similar to that of a high-resolution GCM. In particular, a good correlation between the reconstructed small scales and the reference requires an increase in resolution $\frac{1}{\alpha}$ less than 2 or possibly 3 (Figures 8 and 10). Even if deterministic scores are not important, statistics such as the variance are strongly distorted in our experiments when $\frac{1}{\alpha} \geq 4$. Current nested regional climate models frequently employ grid meshes almost an order of magnitude finer than the GCM serving to drive them. In such a case, if the LAM domain is large and nudging cannot be avoided, indiscriminate nudging will have a strong detrimental effect on the modelled small scales. Scale-selective nudging like spectral nudging might then be a requirement rather than an interesting option.

To summarize, we have evaluated the ability of the dynamical downscaling framework to reconstruct the small scales of the dynamics given its large scales. We find that for a moderate ratio of resolved scales, a large to global model domain and an adequate nudging time, the small scales of the downscaled field achieve a substantial correlation with the small scales of the reference field. For a small LAM domain, the boundary conditions sufficiently control the atmospheric dynamics and low sensitivity is found on the nudging time. In this work we focus on indiscriminate nudging. Spectral nudging is the object of ongoing work. We must stress that we use both statistic and deterministic skill scores to evaluate the RCM. For climate modelling

it is the statistics of the simulations that matters, not the deterministic skill. However, we see that in the Coordinated Downscaling Experiment (CORDEX) programme of the World Climate Research Program (WCRP) (Giorgi *et al.*, 2009) a first phase is the downscaling of meteorological reanalyses over 20 years (1989–2008) using RCMs. One key aspect of this phase is the evaluation of the RCMs. In this context, verifying analysis on a time-by-time, point-by-point basis with gridded observations from satellite or reanalyses also makes sense, so the two ways of evaluating RCMs should be used adequately in a complementary way.

Finally, it must be kept in mind that the simple nature of the QG model does not allow the results to be transposed to real regional modelling. More work has to be conducted with RCM integrating the full complexity of the atmospheric processes, but this is left for the future.

Acknowledgements

We are thankful to F. Codron and R. Laprise for fruitful discussion and the two referees who helped to improve the manuscript significantly. This research has received funding from the ANR-MEDUP project, GIS 'Climat-Environnement-Société' MORCE-MED project, and through ADEME (Agence de l'Environnement et de la Maîtrise de l'Energie) contract 0705C0038.

References

- Alexandru A, De Elia R, Laprise R. 2007. Internal variability in regional climate downscaling at the seasonal scale. *Mon. Weather Rev.* **135**(9): 3221–3238.
- Anthes R. 1974. Data assimilation and initialization of hurricane prediction models. *J. Atmos. Sci.* **31**: 702–719.
- Anthes RA, Kuo YH, Baumhefner DP, Errico RM, Bettge TW. 1985. Predictability of mesoscale atmospheric motions. *Adv. Geophys.* **288**: 159–202.
- Anthes R, Khuo Y, Low-Nam S, Bettge T. 1989. Estimation of skill and uncertainty in regional numerical models. *Q. J. R. Meteorol. Soc.* **115**: 763–806.
- Arakawa A. 1966. Computational design for long-term numerical integration of the equations of fluid motion: two-dimensional incompressible flow. Part 1. *J. Comput. Phys.* **1**(1): 119–143.
- Bhaskaran B, Jones RG, Murphy JM, Noguier M. 1996. Simulations of the Indian summer monsoon using a nested regional climate model: domain size experiments. *Clim. Dynam.* **12**(9): 573–587.
- Biner S, Caya D, Laprise R, Spacek L. 2002. 'Nesting of RCMs by imposing large scales'. In *Research Activities in Atmospheric and Oceanic Modelling*, WMO/TD 987; 73–74.
- Coindreau O, Hourdin F, Haefelin M, Mathieu A, Rio C. 2007. Assessment of physical parameterizations using a global climate model with stretchable grid and nudging. *Mon. Weather Rev.* **135**: 1474–1489.
- Davies HC, Turner RE. 1977. Updating prediction models by dynamical relaxation: an examination of the technique. *Q. J. R. Meteorol. Soc.* **103**(436): 225–245.
- De Elia R, Laprise R, Denis B. 2002. Forecasting skill limits of nested, limited-area models: a perfect-model approach. *Mon. Weather Rev.* **130**(8): 2006–2023.
- Denis B, Côté J, Laprise R. 2002a. Spectral decomposition of two-dimensional atmospheric fields on limited area domains using the discrete cosine transform (DCT). *Mon. Weather Rev.* **130**(7): 1812–1829.
- Denis B, Laprise R, Caya D, Côté J. 2002b. Downscaling ability of one-way nested regional climate models: the Big-Brother experiment. *Clim. Dynam.* **18**(8): 627–646.
- Denis B, Laprise R, Caya D. 2003. Sensitivity of a regional climate model to the resolution of the lateral boundary conditions. *Clim. Dynam.* **20**(2): 107–126.
- Errico R, Baumhefner D. 1987. Predictability experiments using a high-resolution, limited-area model. *Mon. Weather Rev.* **115**: 488–504.

- Genthon C, Krinner G, Cosme E. 2002. Free and laterally nudged Antarctic climate of an atmospheric general circulation model. *Mon. Weather Rev.* **130**: 1601–1616.
- Giorgi F, Jones C, Asrar GR. 2009. Addressing climate information needs at the regional level: the CORDEX framework. *WMO Bull.* **58**(3): 175–183.
- Grell G, Dudhia J, Stauffer D. 1995. 'A description of the fifth-generation Penn State/NCAR mesoscale model (MM5)'. NCAR Technical Note, NCAR/TN-398-STR.
- Haidvogel DB, Held IM. 1980. Homogeneous quasigeostrophic turbulence driven by a uniform temperature gradient. *J. Atmos. Sci.* **37**(12): 2644–2660.
- Hoke JE, Anthes R. 1976. The initialization of numerical models by a dynamic initialization technique. *Mon. Weather Rev.* **104**: 1551–1556.
- Kuo H, Williams R. 1992a. Boundary effects in regional spectral models. *Mon. Weather Rev.* **120**: 2986–2992.
- Kuo H, Williams R. 1992b. Scale-dependent accuracy in regional spectral models. *Mon. Weather Rev.* **126**: 2640–2647.
- Lafore J, Stein J, Asencio N, Bougeault P, Ducrocq V, Duron J, Fischer C, Hèreil P, Mascart P, Masson V, Pinty J, Redelsperger J, Richard E, Vilà-Guerau de Arellano J. 1998. The Meso-NH atmospheric simulation system. Part 1. Adiabatic formulation and control simulation. *Ann. Geophys.* **16**: 90–109.
- Leduc M, Laprise R. 2009. Regional climate model sensitivity to domain size. *Clim. Dynam.* **32**(6): 833–854.
- Li Y, Ménard R, Riishøjgaard L, Cohn S, Rood R. 1998. A study on assimilating potential vorticity data. *Tellus* **50A**: 490–506.
- Lo JC, Yang ZL, Pielke RA. 2008. Assessment of three dynamical climate downscaling methods using the weather research and forecasting (WRF) model. *J. Geophys. Res.* **113**(D9): DOI: 10.1029/2007JD009216.
- Lorenz EN. 1963. Deterministic nonperiodic flow. *J. Atmos. Sci.* **20**(2): 130–141.
- Lucas-Picher P, Caya D, Biner S, Laprise R. 2008. Quantification of the lateral boundary forcing of a regional climate model using an aging tracer. *Mon. Weather Rev.* **136**(12): 4980–4996.
- Miguez-Macho G, Stenchikov G, Robock A. 1992. Spectral nudging to eliminate the effects of domain position and geometry in regional climate model simulations. *J. Geophys. Res.* **109**: D13104, DOI: 10.1029/2003JD004495.
- Murphy A, Epstein E. 1989. Skill scores and correlation coefficients in model verification. *Mon. Weather Rev.* **117**: 572–581.
- Noguer M, Jones R, Murphy J. 1998. Sources of systematic errors in the climatology of a regional climate model over Europe. *Clim. Dynam.* **14**(10): 691–712.
- Nutter P, Stensrud D, Xue M. 2004. Effects of coarsely resolved and temporally interpolated lateral boundary conditions on the dispersion of limited-area ensemble forecasts. *Mon. Weather Rev.* **132**(10): 2358–2377.
- Pielke R, Cotton W, Walko R, Tremback C, Nicholls M, Moran M, Wesley D, Lee T, Copeland J. 1992. A description of the fifth-generation Penn State/NCAR mesoscale model (MM5). *Meteorol. Atmos. Phys.* **49**: 69–91.
- Raluca Rad U, Déqué M, Samuel Somo T. 2008. Spectral nudging in a spectral regional climate model. *Tellus* **60**(5): 898–910.
- Salameh T, Drobinski P, Dubos T. 2010. The effect of indiscriminate nudging time on large and small scales in regional climate modelling: application to the Mediterranean basin. *Q. J. R. Meteorol. Soc.* **136**: 170–182.
- Schraff C. 1997. Mesoscale data assimilation and prediction of low stratus in the Alpine region. *Meteorol. Atmos. Phys.* **64**(1): 21–50.
- Seth A, Giorgi F. 1998. The effects of domain choice on summer precipitation simulation and sensitivity in a regional climate model. *J. Climate* **11**(10): 2698–2712.
- Skamarock W, Klemp J, Dudhia J, Gill D, Barker D, Wang W, Powers J. 2005. 'A description of the advanced research WRF version 2'. NCAR Technical Note, NCAR/TN-468-STR.
- Stauffer C, Seaman N. 1990. Use of four-dimensional data assimilation in a limited-area mesoscale model. Part I. Experiments with synoptic-mesoscale data. *Mon. Weather Rev.* **118**: 1250–1277.
- Tang J, Song S, Wu J. 2010. Impacts of the spectral nudging technique on simulation of the East Asian summer monsoon. *Theor. Appl. Climatol.* **101**: 41–51.
- Thompson P. 1957. Uncertainty in the initial state as a factor in the predictability of large scale atmospheric flow patterns. *Tellus* **9**: 275–295.
- Vallis GK. 1983. On the predictability of quasigeostrophic flow: the effects of beta and baroclinicity. *J. Atmos. Sci.* **40**(1): 10–27.
- Van Tuyl A, Errico R. 1989. Scale interaction and predictability in a mesoscale model. *Mon. Weather Rev.* **117**: 495–517.
- Vannitsem S, Chomé F. 2005. One-way nested regional climate simulations and domain size. *J. Climate* **18**(1): 229–233.
- Vidard PA, Dimet FXL, Piacentini A. 2003. Determination of optimal nudging coefficients. *Tellus* **55**(1): 1–15.
- von Storch H, Langenberg H, Feser F. 2000. A spectral nudging technique for dynamical downscaling purposes. *Mon. Weather Rev.* **128**(10): 3664–3673.
- Vukicevic T, Errico R. 1990. The influence of artificial and physical factors upon predictability estimates using a complex limited-area model. *Mon. Weather Rev.* **118**: 1460–1482.
- Vukicevic T, Paegle J. 1989. Influence of one-way interacting lateral boundary conditions upon predictability of flow in bounded numerical models. *Mon. Weather Rev.* **117**: 340–350.
- Yong L, Richard Ménard D, Lars Peter Riishøjgaard D, Cohn SE, Rood RB. 1998. A study on assimilating potential vorticity data. *Tellus* **50**(4): 490–506.
- Zhang Y, Dulière V, Mote P, Salathé E Jr. 2009. Evaluation of WRF and HADRM mesoscale climate simulations over the U.S. Pacific northwest. *J. Climate* **22**: 5511–5526.